Meltables: Fabrication of Complex 3D Curves by Melting

Andrew O. Sageman-Furnas
University of Göttingen

Nobuyuki Umetani
Autodesk Research

Ryan Schmidt
Autodesk Research

Abstract

We propose a novel approach to fabricating complex 3D shapes via physical deformation of simpler shapes. Our focus is on objects composed of a set of planar beams and joints, where the joints are thin parts of the object which temporarily become living hinges when heated, close to a fixed angle defined by the local shape, and then become rigid when cooled. We call this class of objects *Meltables*. We present a novel algorithm that computes an optimal joint sequence which approximates a 3D spline curve while satisfying fabrication constraints. This technique is used in an interactive Meltables design tool. We demonstrate a variety of Meltables, fabricated with both 3D-printing and standard PVC piping.

1 Introduction

3D-Printing allows for the direct manufacture of complex 3D shapes. However, complications often arise, such as the need for hard-to-remove support structures, or structural weakness caused by anisotropy in the printing process [Umetani and Schmidt 2013]. Similar complications arise in traditional manufacturing, and one potential solution is to manufacture the part in an initial configuration, and then *form* it into the target shape.

In this work we explore the use of *forming* in 3D-printing contexts. Our goal is forming which can be easily designed and fabricated, ideally without any external apparatus. This problem is frequently explored in the context of *self-assembly*, where a common modality is thin planar sheets automatically folding along a network of creases, essentially self-actuated papercraft [An et al. 2014; Peraza-Hernandez et al. 2014; Kwok et al. 2015].

Our approach is to use a network of beams connected by joints. However, rather than physical hinges, our joint is a thin section of rigid plastic - essentially a notch in the beam - that temporarily becomes a *living hinge* when heated. The joint is "closed" when one side of the notch collides with the other, and as a result the shape of the notch defines the *closing angle* of the joint. As the object cools, the living hinge reverts to a rigid state, and the object is assembled. Hence, the rigid object undergoes a one-way shape change under the application of heat. We refer to this class of objects as *Meltables*. Some examples can bee seen in Figure 1.

Meltable joints have nontrivial fabrication constraints, e.g., on the minimum and maximum joint angles. Given an arbitrary 3D space curve, we present a dynamic programming algorithm (Section 3) which finds an optimal Meltable approximation, and an interactive tool for exploring the design space of Meltables. We demonstrate a variety of 3D-printed Meltables (Section 4), and also explore large-scale Meltables based on PVC piping.

(a) (b) (c) (d)

Figure 1: *Meltables are objects composed of joints and beams (a), printed in support-free configurations. When heated, the joints soften and the Meltable can be deformed into a target shape (b), which becomes rigid upon cooling. Heat-shrink materials can be used to automatically close joints (c,d) without human intervention.*

1.1 Related Work

The body of work on folding algorithms and fabrication strategies is extensive, we refer the reader to [Demaine and O'Rourke 2007] for more detailed background. Many works have explored self-actuated folding of planar sheets, one recent example is [An et al. 2014]. Self-assembly via folding of one-dimensional chains is most similar to our work. This has been explored both at the micro-scale using DNA [Douglas et al. 2009] and at macro-scales using 3D-printed structures that shrink or swell in water [Raviv et al. 2014]. Leung et al [2011] showed that any 3D volume can be approximated by folding a 1D chain on a lattice.

Using gravity-induced folding as a forming strategy was explored by Mueller et al [2013], where a laser cutter was used to cut and fold a planar acrylic sheet by heating at joints. Automatic insertion of articulated joints has been explored by many works, such as [Zhou et al. 2014], which then allows folding transformations between two shape configurations.

2 Overview

We define a *Meltable* as a rigid object which undergoes a one-way shape change under the application of heat. This is clearly a large design space. Our focus is on objects that can be designed without precise simulation of thermoplastic deformation, or precise heat control. Instead we emulate a mechanical joint with a temporary living hinge, which allows for design in much the same manner as one would design an object with articulating hinges.

2.1 A Meltable Joint

Our designs consist of masses connected via one-dimensional joints, similar to a linkage. We create a Meltable joint by subtracting a wedge-shape, leaving a thin connecting strip of material on one side (Figure 2). The joint is rigid at room temperature, up to the inherent elasticity of the model material. However, when heated, the thin strip becomes pliable and the wedge can close. Because the surrounding shape is thicker, it stays (relatively) rigid over the short heating time, and hence the effect is that of a *living hinge* which re-

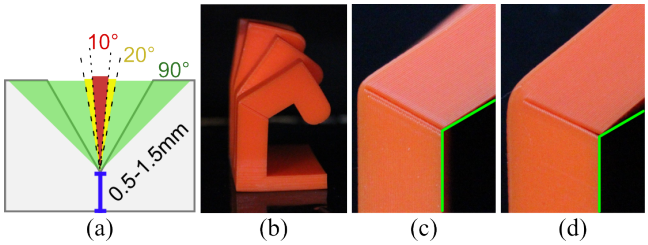

Figure 2: *Parameters ranges (a) of our our meltable joint. Figure (b) shows four bars falling under gravity, with the joint thicknesses* $0.5, 0.75, 1.0, 1.5mm$*. In (c) and (d) the angular error is measured.*

turns to an inflexible state when cooled. If heating is sufficient, the interior sides of the closed joint will bond, however even without this, we find that Meltables are quite strong under compression.

3D-Printed Meltables We 3D-printed Meltables in PLA on a Makerbot Replicator 2, lying flat on the print bed, with the joint notches upwards or downwards. In this configuration the angle can be as small as $10°$, although this is not entirely consistent, and $20°$ is a safer minimum. We do not allow joints wider than $90°$. It is also possible to print shapes vertically with horizontal joint notches. This allows more shape flexibility but adds constraints on the joints, and we found printing vertically to be unreliable.

We varied the joint thickness between 2 layers ($0.5mm$) and 7 layers ($1.5mm$). Thicker joints take longer to soften (Figure 2b), so in self-actuated configurations it is possible to "time" the folding of joints by varying this thickness. As filament strands have some thickness, the joints do not close to the designed angle. This deviation varied from approx $5°$ at $0.5mm$ joints to $10°$ at $1.5mm$.

Large-Scale Meltables 3D-printing is not the only way to fabricate a notched beam. We also explored fabrication of large-scale Meltables with standard PVC piping. We again kept angles in the bounds $[20°, 90°]$, and used the pipe wall thickness as the joint thickness. To create the notches we used a manual fabrication process (ie saw/knife), guided by 3D-printed jigs (Figure 6). We plan to explore an automatic notch-cutting machine in future work.

2.2 Affordances of Meltables

There are few Meltable target shapes which cannot be printed directly (although it is possible to melt into configurations that would be "impossible" to print due to inaccessible support structures). However, physical 3D design involves more than a target shape - physical properties of the final shape are often important, as is fabrication complexity. In this context, Meltables provide a variety of design affordances which can be exploited.

No Support Complex 3D structures often require snap-off *support structures* which waste material, mar the print surface, and in the case of delicate objects, can result in the print being broken when trying to remove the support. A wide range of complex 3D structures can be formulated as Meltables which can be printed without support, and then melted into the target configuration.

Strength In-plane filament strands are stronger than inter-layer bonds. The planar filament lines of a Meltable bend into 3D curves, which can be designed to follow shape stresses. The resulting parts are both stronger and more compliant along certain force directions.

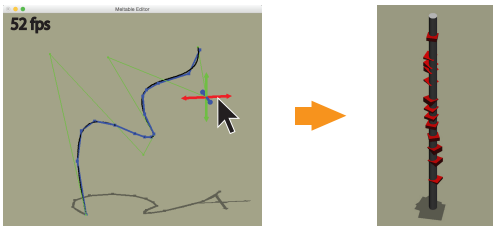

Figure 3: *The Meltable beam user interface (left). The target curve (black) is represented as a spline with control polygon (green). The approximating Meltable predicted shape (blue) is interactively computed against the target curve. Its straight configuration with Meltable joints is shown (right) with its joint wedges (red).*

Reduced Complexity Many Meltables could be fabricated by a multi-component assembly, but the overhead of part management is often significant. For example the Lamp in Figure 6 would involve 25 very similar parts. A single meltable avoids the possibility of misassembly.

2.3 Meltable Design Interface

Our Meltable design tool is shown in Figure 3. The user manipulates a target 3D spline curve, and the system interactively computes a best-approximating 3D-printable Meltable. For PVC-Meltables the software also automatically creates 3D-printable per-joint jigs to aid in manual cutting of the PVC pipe (Figure 6).

3 Method

Our algorithm determines Meltable joint locations, closing angles, and orientations to best approximate a target 3D curve. We achieve interactive rates for finding such optimal Meltable parameters using a dynamic programming approach for curve approximation [Bellman 1961], but here we consider additional fabrication constraints.

To derive a model for Meltables, we assume that the beam has uniform cross section and that each joint is wedge-shaped and symmetric, such that the centers of opposing faces meet exactly when closed. The centerline of the melted shape will then form a polyline $\mathbf{Q} = \{\mathbf{q}_0, \mathbf{q}_1, \ldots, \mathbf{q}_{N+1}\}$, where $\mathbf{q_i} \in \mathbb{R}^3$ and N is the number of joints. The joint fabrication constraints are easily formulated in this model as restrictions on the turning angles of the polyline.

We assume that the target 3D curve $\mathbf{P}$ is given with arclength parameter $0 \leq s \leq s_{end}$, and with position and unit tangent parametrizations $\mathbf{p}(s) \in \mathbb{R}^3$ and $\mathbf{t}(s) = \frac{d\mathbf{p}}{ds}$, respectively. Let the arclengths at the points of a Meltable $\{\mathbf{q}_0, \mathbf{q}_1, \ldots, \mathbf{q}_{N+1}\}$ be given by $\{s_0, s_1, \ldots, s_{N+1}\}$ with $s_0 = 0$ and $s_i < s_{i+1}$. We assume that the Meltable and target curve have the same root point (i.e., $\mathbf{q}_0 = \mathbf{p}(0)$) and the same total length (i.e., $s_{N+1} = s_{end}$). To better approximate the target shape, we further assume they are

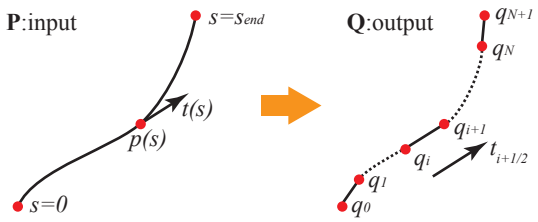

Figure 4: *Notation for a target curve* $\mathbf{P}$ *and Meltable polyline* $\mathbf{Q}$ *that are in tangent correspondence.*

in *tangent correspondence*: at the midpoint of a segment in $\mathbf{Q}$ the tangent of $\mathbf{P}$ should be the same as that of the segment, i.e.,

$$\frac{\mathbf{q}_{i+1} - \mathbf{q}_i}{s_{i+1} - s_i} = \mathbf{t}\left(\frac{s_i + s_{i+1}}{2}\right) = \mathbf{t}_{i+1/2}. \quad (1)$$

A Meltable $\mathbf{Q}$ is then uniquely determined from a sequence of arclengths $\{s_0 = 0, s_1, \ldots, s_N, s_{N+1} = s_{end}\}$ along $\mathbf{P}$ by solving from $\mathbf{q}_0 = \mathbf{p}(0)$ the tangent correspondence equation rewritten as

$$\mathbf{q}_{i+1} = \mathbf{q}_i + (s_{i+1} - s_i)\mathbf{t}_{i+1/2}. \quad (2)$$

Joint Orientation and Constraints For each joint, its closing angle is given by $\theta_i = \arccos(\mathbf{t}_{i-1/2} \cdot \mathbf{t}_{i+1/2})$ and its hinge axis is given by $\boldsymbol{\omega}_i = \mathbf{t}_{i-1/2} \times \mathbf{t}_{i+1/2}$. To understand the orientation of a joint in space we equip $\mathbf{Q}$ with a Bishop frame [Bergou et al. 2008], an adapted twist-free frame found by parallel transporting two orthonormal basis vectors from the root segment. If we denote this frame by $(\mathbf{e}_i^x, \mathbf{e}_i^y, \mathbf{e}_i^z = \mathbf{t}_{i+1/2})$, then a joint i faces in the angle $\mathrm{atan2}(\boldsymbol{\omega}_i \cdot \mathbf{e}_i^y, \boldsymbol{\omega}_i \cdot \mathbf{e}_i^x)$ in the xy-plane of this frame.

As explained in the previous section, there is a constraint on the joint closing angles given by

$$\theta_{min} \leq \theta_i \leq \theta_{max}, \quad i = 1, \ldots, N. \quad (3)$$

We used $\theta_{min} = 20^\circ$ and $\theta_{max} = 90^\circ$ for all our examples. Additionally, neighboring joint wedges must not collide with each other. To prevent collisions we ensure that half the closing width of a joint is less than half the length of its smallest neighboring segment.

$$r\left|\tan\frac{\theta_i}{2}\right| < \min\left\{\frac{s_i - s_{i-1}}{2}, \frac{s_{i+1} - s_i}{2}\right\}, \quad 1 \leq i \leq N, \quad (4)$$

where r is the maximum distance from the beam's cross section boundary to its centerline, e.g., r is the radius for a beam with circular cross section.

Approximation Energy A Meltable polyline is uniquely determined from a sequence of arclengths by solving (2). We use the following energy to choose arclength parameters $\{s_1, \ldots, s_N\}$ so that the resulting Meltable best approximates the target curve, while satisfying the above joint constraints. We define the approximation error of the segment $[s, t]$ of $\mathbf{Q}$ by

$$h(s,t) = \int_s^t ||\mathbf{p}(s) - \mathbf{q}(s)||^2 \, ds, \quad t > s. \quad (5)$$

Furthermore, to penalize invalid joints, $h(s_i, s_{i+1})$ returns $+\infty$ if either the angle constraints (3) or the no-collision constraint (4) for joint angle θ_i is violated. The total energy to minimize is given by

$$E = \sum_{i=0}^{N} h(s_i, s_{i+1}), \quad 0 \leq i \leq N. \quad (6)$$

Observe that $h(s_i, s_{i+1})$ only depends on the parameters $\{s_0, \ldots, s_{i+1}\}$, which allows the following minimization using dynamic programming.

Optimization using Dynamic Programming We find a Meltable polyline $\mathbf{Q}$ close to an input target curve $\mathbf{P}$ by minimizing the approximation energy E with respect to the number of joints N and their arclengths. Note that we need to optimize the number of joints because of our Meltable fabrication constraint — if N is very large or the input curve is close to straight, the joint angles become very small and violate minimum angle constraints.

To make this optimization problem more tractable, we restrict each arclength parameter to be from a finely equally sampled version of the target curve. More precisely, for a large positive integer M and for all $1 \leq i \leq N$ we restrict to s_i in the set $\mathcal{S} = \{\frac{j s_{end}}{M} \mid j = 0, 1, 2, \ldots, M\}$. We also set a maximum number of joints $N \leq N_{max}$. Therefore, we have the following *discrete* optimization:

$$E_{min} = \min_{N,\, s_1, \ldots, s_N} E \quad s.t. \quad \left(\begin{array}{l} s_i \in \mathcal{S},\ s_i < s_{i+1}, \\ 0 \leq i \leq N \leq N_{max} \end{array} \right). \quad (7)$$

Brute force optimization of the approximation energy E is slow since all possible combinations of $\{s_1, \ldots, s_N\}$ in $\mathcal{S}$ must be computed. Namely, this approach has a large computational complexity of order $M^{N_{max}}$. However, the following dynamic programming approach significantly accelerates this process by caching intermediate data. The problem is reduced to computing a table of specially defined subproblems yielding a computational cost of order $M \times N_{max}$. This approach achieves interactive rates for $M = 100$ and $N_{max} = 15$ for single-threaded code on a 2015 MacBook Pro (3GHz core i7 CPU).

For each $0 \leq i \leq N_{max}$ define the function $f_i : \mathcal{S} \to \mathbb{R}$ that returns the best approximation of the target curve from the root s_0 up to s that is split by i number of joints.

$$\begin{aligned} f_0(s) &= h(s_0, s) \quad \text{for} \quad s \in \mathcal{S} \\ f_i(s) &= \min_{s_i < s,\, s_i \in \mathcal{S}} \left(f_{i-1}(s_i) + h(s_i, s)\right) \end{aligned} \quad (8)$$

Dynamic programming accelerates this computation by caching the value $f_i(s)$ once it is computed for some $s \in \mathcal{S}$ and $0 \leq i \leq N_{max}$. The minimum of the approximation energy E for i number of joints is given by $f_i(s_{end})$. The optimal number of joints N is then given by $0 \leq i \leq N_{max}$ that minimize $f_i(s_{end})$. The corresponding arclengths are found by tracing back the sequence of arguments of the minimization of $f_i(s)$ in (8). In practice, we approximate the integral h_i in (5) as a sum of discretely sampled values at $s \in \mathcal{S}$. We also precompute the positions $\mathbf{p}(s)$ and tangents $\mathbf{t}(s)$ for all $s \in \mathcal{S}$ as well as the midpoints of all segments.

4 Results

We designed a wide range of Meltables and performed many experiments. Some examples are shown in Figure 5. These parts were fabricated either horizontally or vertically, without support, and then melted into the configurations shown.

For printed Meltables, we found that heating the PLA to 150°C allowed for manual forming. For automated assembly we focused on gravity-based folding and also closing joints with heat-shrink tubing (attached with pins). In this case there is a trade-off because the lower the temperature, the stiffer the joints, and (particularly at small scales) the part may not have enough mass to fully close the joints. At higher temperatures the joints close easily but the rest of the part may begin to deform. Adding additional masses resolves this complication, as does printing at higher density (ideally solid).

Attaching heat-shrink to close joints adds an additional level of capability (and complexity) to self-assembling Meltables. Correctly placing the strips, which shrink to roughly half their length, was a challenge. We believe this could be automated in the design tool. Figure 6 shows a lamp created using a PVC-Meltable.

As mentioned in Section 2.2, with careful design we can heat-form planar filament loops into 3D curves. This can impart additional strength on the part, as most breakage in 3D-prints occurs when layers de-laminate. Although our notches cut through large portions of the shape, we observed that when they are under compression, the resulting Meltables are often stronger than the directly-printed shape. This is illustrated by experiment in Figure 7.

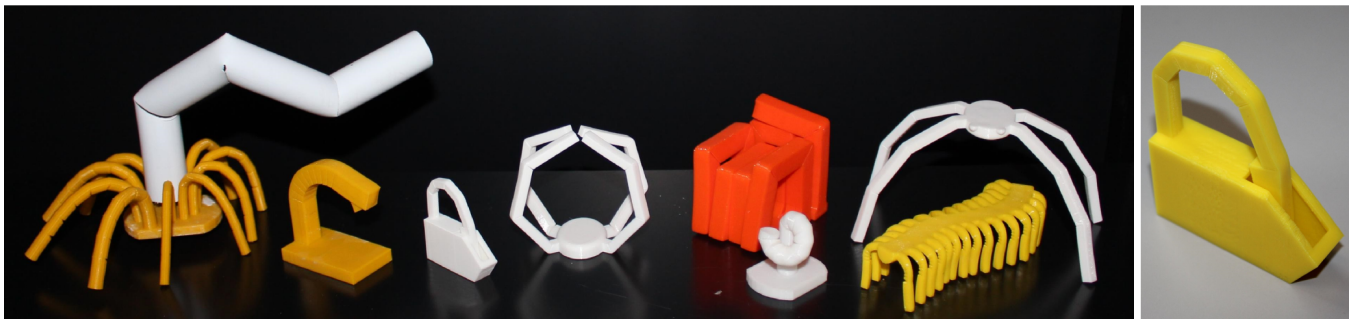

Figure 5: *A menagerie of Meltables. In the figure on the right, the curved portion falls into a cavity. This shape could not be printed directly without the use of inaccessible (and hence unremovable) support structures.*

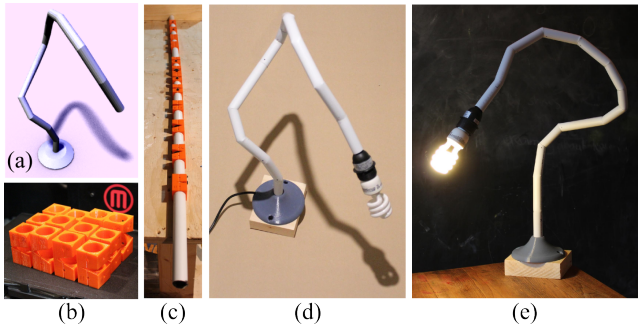

Figure 6: *A Meltable lamp fabricated from a 1.1m section of PVC pipe. Based on the designed curve (a), 3D-printed jigs are generated and used to cut 12 precise notches (b,c). Each joint is heated with a hot-air gun and manually closed to create the lamp arm (d,e).*

4.1 Conclusion

We investigate *Meltables*, shapes composed of planar beams and joints that are heat-formed into more complex configurations via folding at the joints. A novel algorithm and design tool are presented to find Meltable beams which optimally approximate 3D space curves, under fabrication constraints. We explore both manual and automated ("self-") assembly of Meltables, with printed objects and PVC pipes, and demonstrate various benefits, including increased strength, avoidance of support structures in 3D-printing, and creation of objects which would be difficult to print directly.

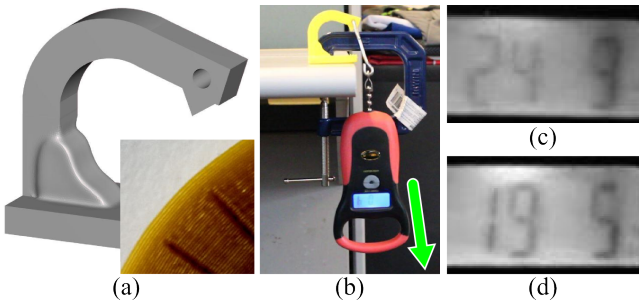

Figure 7: *A Meltable hangar (a) with a* 110° *arc and* $10mm$ *sides contains curved filament strands aligned with the shape (inset). We performed stress-tests (b) by pulling downwards with a simple fishing scale. The Meltable (c) withstands 24.9 pounds (11.3kg), while a print of the target configuration (d) breaks at 19.5 pounds (8.8kg).*

References

AN, B., MIYASHITA, S., TOLLEY, M., AUKES, D., MEEKER, L., DEMAINE, E., DEMAINE, M., WOOD, R., AND RUS, D. 2014. An end-to-end approach to making self-folded 3d surface shapes by uniform heating. In *Proc. ICRA 2014*, 1466–1473.

BELLMAN, R. 1961. On the approximation of curves by line segments using dynamic programming. *Commun. ACM 4*, 6, 284–.

BERGOU, M., WARDETZKY, M., ROBINSON, S., AUDOLY, B., AND GRINSPUN, E. 2008. Discrete elastic rods. *ACM Trans. Graph. 27*, 3, 63:1–63:12.

CHEUNG, K., DEMAINE, E., BACHRACH, J., AND GRIFFITH, S. 2011. Programmable assembly with universally foldable strings (moteins). *IEEE Trans. Robotics 27*, 4, 718–729.

DEMAINE, E., AND O'ROURKE, J. 2007. *Geometric Folding Algorithms: Linkages, Origami, Polyhedra*. Cambridge University Press.

DOUGLAS, S. M., DIETZ, H., LIEDL, T., HOGBERG, B., GRAF, F., AND SHIH, W. M. 2009. Self-assembly of dna into nanoscale three-dimensional shapes. *Nature 459*, 7245, 414–418.

KWOK, T.-H., WANG, C. C., DENG, D., ZHANG, Y., AND CHEN, Y. 2015. 4d printing for freeform surfaces: Design optimization of origami structures. *Journal of Mech. Design*.

MUELLER, S., KRUCK, B., AND BAUDISCH, P. 2013. Laseroriigami: Laser-cutting 3d objects. In *CHI '13 Extended Abstracts*, 2851–2852.

PERAZA-HERNANDEZ, E. A., HARTL, D. J., JR, R. J. M., AND LAGOUDAS, D. C. 2014. Origami-inspired active structures: a synthesis and review. *Smart Mater. Struct. 23*, 9, 094001.

RAVIV, D., ZHAO, W., MCKNELLY, C., PAPADOPOULOU, A., KADAMBI, A., SHI, B., HIRSCH, S., DIKOVSKY, D., ZYRACKI, M., OLGUIN, C., RASKAR, R., AND TIBBITS, S. 2014. Active printed materials for complex self-evolving deformations. *Sci. Rep. 4*.

UMETANI, N., AND SCHMIDT, R. 2013. Cross-sectional structural analysis for 3d printing optimization. In *SIGGRAPH Asia '13 Tech. Briefs*, ACM, 5:1–5:4.

ZHOU, Y., SUEDA, S., MATUSIK, W., AND SHAMIR, A. 2014. Boxelization: Folding 3d objects into boxes. *ACM Trans. Graph. 33*, 4, 71:1–71:8.